



1

2

3

Aerosol concentrations variability over China: two distinct leading modes

4

5

6

Juan Feng¹, Jianlei Zhu^{2,*}, Jianping Li³, and Hong Liao⁴

7

8

1. *College of Global Change and Earth System Science, Beijing Normal University, Beijing,*

9

China

10

2. *Foreign Economic Cooperation Office, Ministry of Ecology and Environment, Beijing, China*

11

3. *Key Laboratory of Physical Oceanography–Institute for Advanced Ocean Studies, Ocean*

12

University of China and Qingdao National Laboratory for Marine Science and Technology,

13

Qingdao 266003, China

14

4. *School of Environmental Science and Engineering, Nanjing University of Information Science*

15

& Technology, Nanjing, China

16

17

18

Corresponding author:

19

Dr. Jianlei Zhu

20

Foreign Economic Cooperation Office, Ministry of Ecology and

21

Environment, Beijing, China

22

Email: zhu.jianlei@fecomee.org.cn

23



24

Abstract

25 Understanding the variability in aerosol concentrations (AC) over China is a scientific
26 challenge and is of practical importance. The present study explored the month-to-
27 month variability in AC over China based on simulations of an atmospheric chemical
28 transport model with a fixed emissions level. The month-to-month variability in AC
29 over China is dominated by two principal modes: the first leading mono-pole mode and
30 the second meridional dipole mode. The mono-pole mode mainly indicates enhanced
31 AC over eastern China, and the dipole mode displays a south-north out-of-phase pattern.
32 The two leading modes are associated with different climatic systems. The mono-pole
33 mode relates to the 3-month leading El Niño-South Oscillation (ENSO), while the
34 dipole mode connects with the simultaneous variation in the North Atlantic Oscillation
35 (NAO) or the Northern Hemisphere Annular Mode (NAM). The associated anomalous
36 dynamic and thermal impacts of the two climatic variabilities are examined to explain
37 their contributions to the formation of the two modes. For the mono-pole mode, the
38 preceding ENSO is associated with anomalous convergence, decreased planetary
39 boundary layer height (PBLH), and negative temperature anomalies, which are
40 unfavorable for emissions. For the dipole mode, the positive NAO is accompanied by
41 opposite anomalies in the convergence, PBLH, and temperature over southern and
42 northern China, paralleling the spatial formation of the mode. This result suggests that
43 the variations originating from the tropical Pacific and extratropical atmospheric
44 systems contribute to the dominant variabilities of AC over China.

45



46 **1. Introduction**

47 Aerosol particles are the primary pollutants in the atmosphere and play significant
48 roles in influencing human health, environmental pollution, and regional and global
49 climate (IPCC, 2013). The variation in aerosols shows considerable impacts on the
50 climate via its direct and indirect effects by altering the radiation forcing and
51 microphysical effects (e.g., Thompson, 1995; Zhang et al., 2011; Huang et al., 2006),
52 indicating the important influences on the regional and global climate. For instance, it
53 is noted that the ‘cooling pool’ in eastern-central China during the period 1960-1990 is
54 partially attributed to increased aerosol concentrations (AC; Li et al., 2016), and that
55 aerosols may exert influences on precipitation changes in both global and regional
56 scales, as well as on monsoon systems (Rosenfeld et al., 2007; Cowan and Cai, 2011;
57 Huang et al., 2014; Jiang et al., 2016; Lou et al., 2018). Thus, a better understanding of
58 the AC variation is of significance for both scientific and practical efforts.

59 Meanwhile, the distribution and accumulation of aerosols are sensitive to
60 meteorological conditions. The variations in the meteorological factors, e.g.,
61 precipitation, wind, temperature, planetary boundary layer height (PBLH), atmospheric
62 stability, and humidity, could impact the AC by modulating the aerosol transport,
63 deposition, and dilution processes (Aw and Kleeman, 2003; Lin and McElroy, 2010;
64 Liao et al., 2015; Yang et al., 2017). The anomalies in meteorological conditions are
65 attributed to the synoptic weather and climate systems. For the synoptic weather scale,
66 Guo et al. (2014) indicated that stagnate weather conditions contribute to the periodic
67 cycle of particulate matter events during boreal winter in Beijing. And the increase in



68 relative humidity (Han et al., 2014) and decrease in the PBLH (Quan et al., 2014; Yang
69 et al., 2015) would lead to an increase in the aerosols, thus contributing to the haze
70 events during winter 2012 in northern China.

71 Meanwhile, the variations in the large-scale climatic systems, such as Pacific
72 Decadal Oscillation (PDO), El Niño-South Oscillation (ENSO), East Asian summer
73 and winter monsoon (EASM & EAWM), and North Atlantic Oscillation (NAO) show
74 considerable effects in impacting the regional AC in both the seasonal and the
75 interannual timescales. For example, researchers found that low values of AC are
76 observed in Taiwan accompanied with the onset of the EASM (Chen and Yang, 2008).
77 During the mature phase of the moderate La Niña event 2000/01, an anomalous south-
78 negative-north-positive AC dipole pattern is seen over eastern China (Feng et al., 2017).
79 The interannual variations in the EASM exhibit significant effects in impacting the
80 summertime AC over China, i.e., high-level AC would be observed over eastern China
81 along with a weaker EASM (Zhu et al., 2012; Lou et al., 2016; Mao et al., 2017). A
82 similar situation is observed between the EAWM and AC over eastern China but during
83 boreal winter, showing that a weaker EAWM relates to a high level of AC over China
84 (Jeong et al., 2017). Zhao et al. (2016) have indicated that the decadal regime shift of
85 the PDO showed significant role in impacting the decadal variations of boreal winter
86 aerosols over eastern China. Feng et al. (2019) have reported the important influences
87 of simultaneous ENSO and preceding autumn NAO signals on the winter AC over
88 China by case study.



89 The above discussions highlight the effect of climate background in impacting the
90 AC over China across different seasons, including signals from both the tropical and
91 the extratropical, and originating from both the atmosphere and the ocean. However,
92 the relative roles of climate systems are still unknown because there are strong
93 interactions among the systems. For example, during the decaying summer of a warm
94 ENSO event, a weaker EASM is expected to be observed (Wu et al., 2002), and the
95 occurrence of a cold ENSO event during its mature phase is favorable for a stronger
96 EAWM (Wang et al., 2008). The preceding spring (March to April) NAO indicates
97 significant impacts on the following summer EASM in the interannual timescale (Wu
98 et al., 2009). Moreover, the signals originating from the atmosphere (e.g., NAO, EASM,
99 EAWM) and ocean (e.g., ENSO, PDO) present strong seasonality, prevailing in
100 different seasons. As shown by the fact that AC over China are impacted by various
101 climate systems, the relative importance of individual signals on their possible impacts
102 in modulating the variability of AC remains unknown. Meanwhile, most of the previous
103 studies regarding the influence of climate systems on AC focused on a certain season
104 with little attention paid to spatial-temporal variability. These questions are important
105 for improving the recognition of the modulation of climate systems on AC.

106 Consequently, one of the crucial motivations of the current work is to investigate
107 the spatial-temporal variability in the monthly AC over China, highlighting the potential
108 effects of climatic variabilities in modulating the spatial and temporal variations in AC,
109 and understanding the possible physical processes involved. The rest of the study is
110 arranged as follows. The model, datasets, and methods are presented in Section 2; The



111 properties of the leading modes of AC variability are described in Section 3; Section 4
112 discusses the contribution of climatic modes on aerosol variabilities; and Section 5
113 provides the conclusions and discussions.

114 **2. Datasets, model, and methodology**

115 **2.1 Model**

116 The GEOS-Chem model is employed to detect the variability in AC over China.
117 This model is a 3-dimensional tropospheric chemistry model with a 2.5° longitude \times 2°
118 latitude horizontal resolution and 30 vertical levels. The model is widely applied to
119 investigate the potential modulation of climatic variabilities on the anomalous
120 distributions of pollutants on various timescales, for example, on the seasonal
121 (Generoso et al., 2008; Jeong et al., 2011; Feng et al., 2019), interannual (Jeong et al.,
122 2017; Li et al., 2019), and interdecadal (Zhu et al., 2012) timescales. The high
123 consistency in both the temporal and spatial distributions between the simulations and
124 observations provides confidence for the feasibility of the present study.

125 As reported, the significant upward trend in anthropogenic emissions over China
126 accounts for a large variance in pollutants, and the first dominant mode of boreal winter
127 aerosols over eastern China represents anthropogenic emissions (Zhao et al., 2016). To
128 highlight the modulation of the climatic variabilities on the variation in the aerosols,
129 the anthropogenic and biomass burning emissions have been fixed at the year 2005
130 level. Thus, the variations in the aerosols in this context are attributed to the internal
131 climatic variability.



132 The definition of particulate matter smaller than 2.5 μm in diameter (PM_{2.5}) is
133 followed by Liao et al. (2007),

$$134 \quad [PM_{2.5}] = 1.29 \times [NO_3^-] + 1.37 \times [SO_4^{2-}] + [SOA] + [POA] + [BC]$$

135 where NO_3^- , SO_4^{2-} , SOA, POA, and BC are the aerosol particles of nitrate, sulfate,
136 secondary organic aerosol, primary organic aerosol, and black carbon, respectively.
137 Mineral dust and sea salt are excluded because these species are not the major
138 components over China.

139 2.2 Datasets and methodology

140 The input meteorological variables of the model highly agree with the widely used
141 atmospheric and oceanic datasets, i.e., the National Centers for Environmental
142 Prediction/National Center for Atmospheric Research (NCEP/NCAR) reanalysis
143 (Kalnay et al., 1996), and the UK Meteorological Office Hadley Centre's sea ice and
144 sea surface temperature (SST) datasets (HadISST; Rayner et al., 2003). These two
145 datasets are employed to verify the climatic indices calculated based on the model input
146 meteorological datasets. ENSO was characterized by the Niño 3.4 index, which is
147 defined as the areal averaged SST over 120°W-170°W, 5°N-5°S. The monthly Niño 3.4
148 indices based on the HadISST and model input data are highly related with each other
149 with a correlation coefficient of 0.99, confirming the reliability of the model data. The
150 North Atlantic Oscillation index (NAOI) and Northern Hemisphere Annular Mode
151 index (NAMI) are used to present the sea level pressure (SLP) oscillation between the
152 mid-latitudes and high latitudes in the extratropical Northern Hemisphere. Following



153 Li and Wang (2003), the NAMI is defined as the difference in the normalized global
154 zonal-mean SLP between 35°N and 65°N, in which the 35°N and 65°N refer to the mid-
155 latitude and high latitude, respectively. The definition of the NAOI resembles that of
156 the NAMI but within the North Atlantic sector from 80°W to 30°E. Because the NAOI
157 and NAMI are highly correlated with each other in both spatial distribution and
158 temporal variation (Thompson and Wallace, 1998; Gong et al., 2001), the NAOI is
159 utilized in the current context; similar results are obtained based on the NAMI.

160 Empirical orthogonal function (EOF) analysis was employed to obtain the
161 spatiotemporal variability in monthly PM_{2.5} over China. Correlation and regression are
162 used to display the linkages between the variability in the PM_{2.5} and the climatic modes.
163 Here, the period 1986–2006 was taken as the climatological mean, and the annual cycle
164 was removed before the analyses.

165 **3. Distinct leading modes of the variability in aerosol concentrations**

166 **3.1 Two leading modes**

167 Figure 1 presents the spatial distribution of the first (EOF1) and second (EOF2)
168 leading modes based on the monthly surface layer and column AC anomalies. A similar
169 spatial distribution is observed in both the surface and column AC. The EOF1 and EOF2
170 modes explain 31.4% (37.0%) and 16.3% (14.1%) of the total variances for the surface
171 layer (column) AC, respectively. Based on the *North's* rule, the two dominant modes
172 could be significantly separated from each other and from the rest of the eigenvectors
173 based on the analysis of the eigenvalues in the light of sampling error above the 0.05



174 significance level. The rest of the modes are not discussed for their relative less
175 explained variance or could not be well separated. The EOF1 mode displays a mono-
176 sign pattern, with the maximum located in central eastern China (Figs. 1a and c). The
177 EOF2 mode presents a meridional dipole pattern in eastern China, with opposite values
178 to the south (positive values) and north (negative values) of the Yangtze River.

179 The temporal behavior of the two modes, the first and second principal
180 components, i.e., PC1 and PC2, is displayed in Figure 2. Both PC1 and PC2 show strong
181 interannual variations. The PCs based on the surface and column concentrations are
182 closely correlated with each other, with coefficients of 0.80 and 0.79 for PC1 and PC2,
183 respectively. The high consistency between the surface and column concentrations in
184 both the spatial and temporal distributions implies that the factors governing their
185 variations are the same. The maximum value of PC1 occurs in 1998, corresponding to
186 the strongest El Niño event (1997/98) in the 20th century. For PC2, negative values are
187 observed during the winters of 1989 and 2002, and positive values are observed during
188 the winters of 1995 and 1997. However, the winters of 1989 and 2002 correspond to
189 the positive polarities of the NAM or NAO, and the winters of 1995 and 1997 are
190 paralleling to the negative polarities of the NAM or NAO. The potential linkage
191 between the PCs and climatic variabilities is therefore analyzed. Here, the Niño 3.4
192 index is utilized to depict the variation of ENSO, and the NAOI (NAMI) is employed
193 to reflect the variability in the NAO (NAM). Note that the indices based on the model
194 input data are highly correlated with the observation datasets, and the monthly NAOI
195 is closely related with the NAMI, exhibiting a significant correlation coefficient of 0.71



196 during period 1986-2006. Therefore, the NAOI is employed to detect the linkage
197 between the PC2 and climate variability.

198 **3.2 Linkage with the climate variabilities**

199 Figure 3 displays the lead-lag correlation between the PC1 and Niño 3.4 index,
200 and between the PC2 and NAOI to identify the linkage between the climatic
201 variabilities and the two leading AC patterns. PC1 is significantly connected with the
202 Niño 3.4 index, with the maximum occurring when the Niño 3.4 index is 3 months
203 leading, implying a leading influence on PC1. The leading impacts of Niño 3.4 on the
204 variation in PC1 are further seen from the seasonal evolution of the standard deviation
205 in the corresponding indices (Fig. 4). The standard deviation of the monthly Niño 3.4
206 index shows that the maximum occurs during December, while the maximum occurs in
207 March for that of PC1. The leading influences of Niño 3.4 on PC1 are further verified
208 by the spatial distribution of correlations between PC1 and SST, as shown in Figure 5.
209 For the correlation with the PC1 lagged for 3 months, significant positive correlations
210 are observed over the tropical eastern Pacific and Indian Oceans, and negative
211 correlations over the tropical western Pacific. The correlation pattern is like a canonical
212 El Niño pattern. Note that the significant positive correlations over the tropical eastern
213 Pacific gradually decrease as the SST leading time is reduced; however, the correlations
214 over the tropical Indian Ocean become stronger, implying the effects of the Indian
215 Ocean capacitor along with the development of an ENSO event (Xie et al., 2009). The
216 above result ascertains the preceding influence of ENSO on the variation in PC1,
217 indicating a 3-month leading impact of ENSO on the following AC over China.



218 Meanwhile, the maximum negative correlation between PC2 and the NAO is
219 simultaneous (Fig. 3b), implying a simultaneous impact of the NAO on the AC over
220 China. Similar result is seen in the correlation between the NAMI and PC2. The
221 simultaneous relationship between the PC2 and NAO is further estimated in their
222 corresponding seasonal variation in the standard deviation (Figs. 4b and d). The
223 maximum standard deviations of the NAO and PC2 both occur during January-
224 February-March. A similar result is obtained based on the NAMI, suggesting significant
225 negative impacts of the extratropical atmosphere variation on the AC over eastern China.
226 Moreover, the correlations between the simultaneous PC2 and SLP display a negative
227 NAO-like (NAM-like) structure, with significant positive correlations over the polar
228 regions and negative correlations over the mid-latitudes. Note that this anomalous
229 pattern is consistently observed in PC2s based on both the surface layer and the column
230 concentrations.

231 The result above suggests that the variability in AC can be measured by climatic
232 variabilities, of which the variation in EOF1 is linked to the 3-month leading SST
233 variation over the tropical eastern Pacific, and that of EOF2 is related to the
234 extratropical atmospheric variability-NAO. The possible physical process involved in
235 their relationship is discussed in the following section.

236 **4. Physical processes impacting on the leading modes**

237 **4.1 Circulation anomalies associated with ENSO**



238 Figure 7 shows the anomalous circulations associated with ENSO to identify the
239 atmospheric circulation process impacting the EOF1 patterns with the Niño 3.4 index
240 leading for 3 months. It is seen that tropical eastern Pacific and southern China are
241 controlled by significant positive correlations in the correlation with the divergence in
242 the lower troposphere. That is, southern China and tropical eastern Pacific are
243 influenced by anomalous convergence circulation under the influence of a 3-month
244 leading ENSO signal. Meanwhile, tropical western Pacific is impacted by significant
245 negative correlations, indicating that these regions are impacted by anomalous
246 divergence. The anomalous convergence circulation over southern China is not
247 favorable for the emission of AC. That is the anomalous circulation associated with 3-
248 month leading ENSO signal would connect with enhanced AC over eastern China,
249 which agrees with the spatial distribution of EOF1. Moreover, the impacts of ENSO on
250 the circulation is further seen in impacting the PBLH (Figure 8a). Significant negative
251 correlations are found over eastern China, indicating that the occurrence of a warm
252 ENSO event would decrease the height of PBLH. The decreased PBLH relates to
253 enhanced AC over eastern China. The above result suggests that the leading ENSO
254 signal exhibits a significant role in affecting the circulation anomalies over China.
255 Under the influence of warm ENSO events, the followed anomalous convergence and
256 decreased PBLH over eastern China are both unfavorable for the emission of AC,
257 contributing to the formation of the EOF1 pattern.

258 **4.2 Circulation anomalies associated with NAO**



259 The anomalous divergence accompanied by the simultaneous NAO is presented in
260 Figure 9. The northern Atlantic Ocean is influenced by an anomalous tripole structure,
261 showing convergence-divergence-convergence anomalies from the polar region to the
262 tropical regions. The occurrence of the anomalous circulation structure in the northern
263 Atlantic Ocean is due to the fact that the variation in NAO would induce an anomalous
264 tripole SST pattern within the northern Atlantic Ocean (e.g., Wu et al., 2009; Zheng et
265 al., 2016) by which a downstream wave-train is expected to be observed (Ruan et al.,
266 2015; Li and Ruan, 2018). The downstream wave train is seen with significant positive
267 anomalies over southern China in the regression of NAOI to the divergence, while
268 negative anomalies occur over northern China. That is, a positive NAO is accompanied
269 with anomalous divergence (convergence) over southern (northern) China. The
270 anomalous convergence over northern China is unfavorable for the emission of AC,
271 corresponding to enhanced AC. However, the opposite situation is observed over
272 southern China. The anomalous circulation connected with NAO further estimates the
273 negative impacts of NAO on the EOF2 mode.

274 In addition, the potential impacts of NAO on PBLH over China are further
275 examined. Figure 8b shows the anomalous PBLH regressed with reference to the NAOI
276 to identify the role of NAO in determining the EOF2 mode. For a positive NAO phase,
277 negative PBLH anomalies occupy northern China, suggesting a favorable condition for
278 enhanced AC. In contrast, southern China is controlled by positive PBLH anomalies,
279 paralleling the situation for decreased AC. The circulation anomalies connected with
280 NAO in both the divergence and PBLH suggest that the impacts of NAO on the AC



281 over northern and southern China are opposite, consistent with the spatial distribution
282 of the EOF2 mode.

283 **4.3 Role of temperature**

284 Meanwhile, it has been reported that temperature shows an effect in impacting the
285 distribution of aerosols. For example, it is reported that an increase in temperature is
286 associated with a decrease in PM_{2.5} over southern California (Aw and Kleeman, 2003)
287 because enhanced temperature lead to decreases in organics and nitrate (Dawson et al.,
288 2007). Accordingly, the associated impacts of the ENSO and NAO on the temperature
289 over China are detected. Figure 10 displays the anomalous temperature regressed
290 against the 3 months preceding Niño 3.4 index and simultaneous NAOI to detect the
291 temperature anomalies connected with the two climate systems. For a warm event of
292 ENSO, large areas of negative temperature anomalies occupy eastern China, with the
293 maximum lying within the Yellow River and Yangtze River (Fig. 10a). The negative
294 temperature anomalies imply a lower temperature condition, which would induce to
295 enhanced AC.

296 For the NAO, its positive phase corresponds to opposite temperature anomalies
297 over southern and northern China, being positive (negative) over the southern (northern)
298 China (Fig. 10b). Positive temperature anomalies over southern China parallels to a
299 warmer situations and reduced AC in this region. Negative temperature anomalies over
300 northern China set up a background of colder situations, which would increase the AC.
301 The anomalous variation in the temperature agrees with the negative impact of NAO



302 on the AC over eastern China. In addition, the temperature anomalies accompanied with
303 the preceding ENSO are greater than those associated with the simultaneous NAO,
304 highlighting the dominant role of ENSO in impacting the AC over eastern China.

305 **5. Conclusions and Discussions**

306 China has a high loading of aerosols and understanding the variability in AC is
307 important not only for recognizing the interactions between aerosols and climate but
308 also for scientifically understanding the current pollutant status. In the present work, it
309 is shown that the month-to-month AC over China are dominated by two principal
310 modes: the mono-pole mode and the meridional dipole mode. The first mono-pole mode
311 mainly exhibits the enhanced AC pattern over eastern China. The dipole mode shows
312 two centers over northern and southern China, with positive (negative) values over
313 southern (northern) China. The potential linkages between the two modes and climatic
314 sources are further described. The first mono-pole mode is linked with the 3 months
315 preceding ENSO, and the second dipole mode is connected with the simultaneous NAO.

316 The possible physical mechanism is also investigated by examining the dynamic
317 and thermal processes involved. For the mono-pole mode, the preceding ENSO can
318 induce anomalous convergence and decrease PBLH over eastern China, which are not
319 favorable for the emission of AC. Meanwhile, it is seen that anomalous negative
320 temperature over eastern China are seen accompanied with the preceding ENSO events,
321 paralleling conditions favorable for enhanced AC. For the meridional dipole mode,
322 anomalous convergence (divergence) and decreased (increased) PBLH are found over



323 northern (southern) China, paralleling the conditions for increased (decreased) AC
324 under the positive phase of NAO. Moreover, the temperature anomalies associated with
325 the NAO over southern and northern China are opposite, agreeing well with the spatial
326 distribution of the dipole mode. That is, both the dynamic and thermal anomalies
327 associated with climate systems are contributed to formation of the leading variabilities
328 of AC over China.

329 On the other hand, as reported, wet deposition shows important effects in
330 influencing the anomalous distribution of AC (Wu, 2014). However, the role of wet
331 deposition is not discussed in the present work. This is because the influences of ENSO
332 on the seasonal rainfall over China is complex and vary along with the phases of ENSO
333 events. During the decaying summer of a warm ENSO event, above average rainfall is
334 expected to be observed over southern China (e.g., Huang and Wu, 1989; Feng et al.,
335 2016); however, this is not the case for the developing summer (Feng et al., 2016).
336 Moreover, when the intensities of the ENSO events are different, i.e., moderate events
337 vs. strong events, their impacts on the seasonal rainfall over China may vary differently
338 (Xue and Liu, 2008). In addition, it has been indicated that the influence of rainfall on
339 the aerosols exhibits seasonal and regional dependence (Wu, 2014), and it is found that
340 the role of rainfall is limited in affecting the winter aerosols over southern China (Wu,
341 2014). However, the month-to-month variability of AC is considered in this study,
342 whereas for a specific season, the potential impacts of wet deposits in determining the
343 distribution of aerosols is complex and uncertainties exist.

344 Furthermore, the characteristics of the month-to-month variability of aerosols over



345 China is explored, the result highlights the impacts of tropical SST (i.e., ENSO) and the
346 atmospheric system (i.e., NAO or NAM) originating from the Northern Hemisphere on
347 the variability in AC over China. As reported, both ENSO and NAO display
348 considerable influences on the climate anomalies over China (e.g., Huang and Wu, 1989;
349 Zhang et al., 1996; Gong and Wang, 2003; Li and Wang, 2003), and the result here
350 expands their influences beyond climate. Climate systems, for example, originating
351 from the Southern Hemisphere, display essential influences in affecting seasonal
352 rainfall and temperature anomalies via atmospheric bridges and oceanic bridges (Zheng
353 et al., 2015, 2018). Future work will further examine the potential impacts of the
354 Southern Hemisphere climate systems on the variation in AC over China to
355 comprehensively assess the modulations of climate systems on the AC over China.

356



357 ***Author contribution***

358 JLZ and JF conducted the study design. JLZ performed the simulations. JF and
359 JLZ carried out the data analysis. JPL and HL were involved in the scientific
360 interpretation. JF prepared the manuscript with contributions from all coauthors.

361 ***Data availability***

362 The HadISST dataset are downloaded from
363 <http://www.metoffice.gov.uk/hadobs/hadisst/data/download.html>. The NCEP/NCAR
364 reanalyses is downloaded from <http://www.esrl.noaa.gov/psd/data/gridded/>. Simulation
365 results and codes to generate figures in this paper have been archived by corresponding
366 authors and are available at <https://doi.org/10.5281/zenodo.3247326>.

367 ***Acknowledgements***

368 This research has been supported by the National Natural Science Foundation of
369 China (grant nos. 41790474, 41705131, and 41975079).

370



371 **References**

- 372 Aw, J., and Kleeman, M. J.: Evaluating the first-order effect of intra-annual temperature
373 variability on urban air pollution, *J. Geophys. Res. Atmos.*, 108, D12, 4365,
374 <https://doi.org/10.1029/2002JD002688>, 2003.
- 375 Chen, B. Q., and Yang, Y. M.: Remote sensing of the spatio-temporal pattern of aerosol
376 over Taiwan Strait and its adjacent sea areas, *Acta Scientiae Circumstantiae*, 28,
377 2597-2604, 2008.
- 378 Cowan, T., and Cai, W. J.: The impact of Asian and non-Asian anthropogenic aerosols
379 on 20th century Asian summer monsoon, *Geophys. Res. Lett.*, 38, L11703,
380 <https://doi.org/10.1029/2011GL047268>, 2011.
- 381 Dawson, J. P., Adams, P. J., and Pandis, S. N.: Sensitivity of PM_{2.5} to climate in the
382 Eastern US: a modeling case study, *Atmos. Chem. Phys.*, 7, 4295-4309, 2007.
- 383 Feng, J., Li, J. P., Zheng, F., Xie, F., and Sun, C.: Contrasting impacts of developing
384 phases of two types of El Niño on southern China rainfall, *J. Meteorol. Soc. Jap.*,
385 94, 359-370, <https://doi.org/10.2151/jmsj.2016-019>, 2016.
- 386 Feng, J., Li, J. P., J. Zhu, J. L., Liao, H., and Yang, Y.: Simulated contrasting influences
387 of two La Niña Modoki events on aerosol concentrations over eastern China, *J.*
388 *Geophys. Res. Atmos.*, 122, <https://doi.org/10.1002/2016JD026175>, 2017.
- 389 Feng, J., Li, J. P., Liao, H., and Zhu., J. L.: Simulated coordinated impacts of the
390 previous autumn North Atlantic Oscillation (NAO) and winter El Niño on winter
391 aerosol concentrations over eastern China, *Atmos. Chem. Phys.*, 19, 10787-10800,
392 <https://doi.org/10.5194/acp-19-10787-2019>, 2019.



- 393 Generoso, S., Bey, I., Labonne, M., and Breon, F. M.: Aerosol vertical distribution in
394 dust outflow over the Atlantic: Comparisons between GEOS - Chem and Cloud -
395 Aerosol Lidar and Infrared Pathfinder Satellite Observation (CALIPSO), J.
396 Geophys. Lett. Atmos., 113, D24209, <https://doi.org/10.1029/2008JD010154>,
397 2008.
- 398 Gong, D. Y., Wang, S. W.: Influence of Arctic Oscillation on winter climate over China,
399 J. Geogr. Sci., 13, 208-216,
400 <https://xs.scihub.ltd/https://doi.org/10.1007/BF02837460>, 2003.
- 401 Gong, D. Y., Wang, S. W., and Zhu, J. H., East Asian Winter Monsoon and Arctic
402 Oscillation, Geophys. Res. Lett., 28, 2073-2076,
403 <https://doi.org/10.1029/2000GL012311>, 2001.
- 404 Guo, S., Hu, M., Zamora, M. L., Peng, J. F., Shang, D. J., Zheng, J., Du, Z. F., Wu, Z.
405 J., Shao, M., Zeng, L. M., Molina, M. J., and Zhang, R. Y.: Elucidating severe
406 urban haze formation in China, PNAS, 111, 17373-17378,
407 <https://doi.org/10.1073/pnas.1419604111>, 2014.
- 408 Han, S. Q., Wu, J. H., Zhang, Y. F., Cai, Z. Y., Feng, Y. C., Yao, Q., Li, X. J., Liu, Y. W.,
409 Zhang, M., Characteristics and formation mechanism of a winter haze-fog episode
410 in Tianjin, China, Atmos. Environ., 98, 323-330.
411 <https://doi.org/10.1016/j.atmosenv.2014.08.078>, 2014.
- 412 Huang, J. P., Lin, B., Minnis, P., Wang, T., Wang, X., Hu, Y., Yi, Y., and Ayers, J. R.:
413 Satellite-based assessment of possible dust aerosols semi-direct effect on cloud



414 water path over East Asia, *Geophys. Res. Lett.*, 33,
415 <https://doi.org/10.1029/2006GL026561>, 2006.

416 Huang, J. P., Wang, T., Wang, W., Li, Z., and Yan, H.: Climate effects of dust aerosols
417 over East Asian arid and semiarid regions, *J. Geophys. Res. Atmos.*, 119398–
418 11416, <https://doi.org/10.1002/2014JD021796>, 2014.

419 Huang, R. H., and Y. F. Wu: The influence of ENSO on the summer climate change in
420 China and its mechanism, *Adv. Atmos. Sci.*, 6, 21-32,
421 <https://xs.scihub.ltd/https://doi.org/10.1007/BF02656915>, 1989.

422 IPCC, *Climate change.: The physical science basis*. Cambridge University Press.
423 Cambridge, UK, 2013.

424 Jeong, J. I., Park, R. J., Woo, J. H., Han, Y. J., and Yi, S. M.: Source contributions to
425 carbonaceous aerosol concentrations in Korea, *Atmos. Environ.*, 45, 1116-1125,
426 <https://doi.org/10.1016/j.atmosenv.2010.11.031>, 2011.

427 Jeong, J. I., and Park, R. J.: Winter monsoon variability and its impacts on aerosol
428 concentrations in East Asia, *Environ. Poll.*, 221, 285-292,
429 <https://doi.org/10.1016/j.envpol.2016.11.075>, 2017.

430 Jiang, Z. H., Huo, F., and Ma, H. Y., Impact of Chinese Urbanization and Aerosol
431 Emissions on the East Asian Summer Monsoon, *J. Climate*, 30, 1019-1039,
432 <https://doi.org/10.1175/JCLI-D-15-0593.1>, 2016.

433 Kalnay, E., Kanamitsu, M., Kistler, R., Colliins, W., Deaven, D., Gandin, L., Iredell,
434 M., Saha, S., White, G., Woollen, J., Zhu, Y., Chelliah, M., Ebisuzaki, W., Higgins,
435 W., Janowiak, J., Mo, K. C., Ropelewski, C., Wang, J., Leetmaa, A., Reynolds, R.,



- 436 Jenne, R., and Joseph, D.: The NCEP/NCAR 40-Year Reanalysis Project, Bull.
437 Amer. Meteor. Soc., 77, 437-472, [https://doi.org/10.1175/1520-](https://doi.org/10.1175/1520-0477(1996)077<0437:TNYRP>2.0.CO;2)
438 [0477\(1996\)077<0437:TNYRP>2.0.CO;2](https://doi.org/10.1175/1520-0477(1996)077<0437:TNYRP>2.0.CO;2), 1996.
- 439 Li, J. P., and Ruan, C. Q.: The North Atlantic–Eurasian teleconnection in summer and
440 its effects on Eurasian climates. Environ. Res. Lett., 13,
441 <https://doi.org/10.1088/1748-9326/aa9d33>, 2018.
- 442 Li, J. P., and Wang, J. X. L.: A new North Atlantic Oscillation index and its variability,
443 Adv. Atmos. Sci., 20, 661-676, <https://doi.org/10.1007/BF02915394>, 2003.
- 444 Li, K., Jacob, D. J., Hong, L., Zhu, J., Shah, V., Shen, L., Bates, K. H., Zhang, Q., and
445 Zhai, S. X.: A two-pollutant strategy for improving ozone and particulate matter
446 air quality in China, Nature Geoscience, 12, 906-910,
447 <https://doi.org/10.1038/s41561-019-0464-x>, 2019.
- 448 Li, Z. Q., Lau, W. K., Ramanathan, V., et al.: Aerosol and monsoon climate interactions
449 over Asia. Rev. Geophys., 54, 866–929, <https://doi.org/10.1002/2015RG000500>,
450 2016.
- 451 Liao, H., Henze, D. K., Seinfeld, J. H., Wu, S. L., and Mickley, L. J.: Biogenic
452 secondary organic aerosol over the United States: Comparison of climatological
453 simulations with observations, J. Geophys. Res., 112,
454 <https://doi.org/10.1029/2006JD007813>, 2007.
- 455 Liao, H., Chang, W., and Yang, Y.: Climatic effects of air pollutants over China: A
456 review, Adv. Atmos. Sci., 32, 115-139, doi:10.1007/s00376-014-0013-x, 2015.



- 457 Lin, J. T., and McElroy, M. B.: Impacts of boundary layer mixing on pollutant vertical
458 profiles in the lower troposphere: Implications to satellite remote sensing. *Atmos.*
459 *Environ.*, 44, 1726–1739, <https://doi.org/10.1016/j.atmosenv.2010.02.009>, 2010.
- 460 Lou, S. J., Russell, L. M., Yang, Y., Xu, L., Lamjiri, M. A., DeFlorio, M. J., Miller, A.
461 J., Ghan, S. J., Liu, Y., and Singh, B.: Impacts of the East Asian Monsoon on
462 springtime dust concentrations over China, *J. Geophys. Res. Atmos.*, 121, 8137-
463 8152, <https://doi.org/10.1002/2016JD024758>, 2016.
- 464 Lou, S. J., Yang, Y., Wang, H. L., Smith, S. J., Qian, Y., Rasch, P. J.: Black carbon
465 amplifies haze over the North China Plain by weakening the East Asian winter
466 monsoon, *Geophys. Res. Lett.*, 45, <https://doi.org/10.1029/2018GL080941>, 2018.
- 467 Mao, Y. H., Liao, H., and Chen H. S.: Impacts of East Asian summer and winter
468 monsoons on interannual variations of mass concentrations and direct radiative
469 forcing of black carbon over eastern China, *Atmos. Chem. Phys.*, 17, 4799-4816,
470 <https://doi.org/10.5194/acp-17-4799-2017>, 2017.
- 471 Quan, J. N., Tie, X. X., Zhang, Q., Liu, Q., Li, X., Gao, Y., Zhao, D. L.: Characteristics
472 of heavy aerosol pollution during the 2012-2013 winter in Beijing, China. *Atmos.*
473 *Environ.*, 88, 83-89. <https://doi.org/10.1016/j.atmosenv.2014.01.058>, 2014.
- 474 Rayner, N. A., Parker, D. E., Horton, E. B., Folland, C. K., Alexander, L. V., and Rowell,
475 D. P.: Global analyses of sea surface temperature, sea ice, and night marine air
476 temperature since the late nineteenth century, *J. Geophys. Res.*, 108, D14, 4407,
477 <https://doi.org/10.1029/2002JD002670>, 2003.



- 478 Rosenfeld, D., Dai, J., Yu, X., Yao, Z. Y., Xu, X. H., Yang, X., and Du, C. L.: Inverse
479 relations between amounts of air pollution and orographic precipitation, *Science*,
480 315, 1396-13398, doi: 10.1126/science.1137949, 2007.
- 481 Ruan, C. Q., Li, J. P., and Feng, J.: Statistical downscaling model for late-winter rainfall
482 over southwest China. *Science China: Earth Sciences*, 58(10), 1827-1839,
483 <https://xs.scihub.ltd/https://doi.org/10.1007/s11430-015-5104-8>, 2015.
- 484 Thompson, R. D., The impact of atmospheric aerosols on global climate: a review, *Prog.*
485 *Phys. Geog.*, 19, 336-350, <https://doi.org/10.1177/030913339501900303>, 1995.
- 486 Thompson, D. W. J., and Wallace, J. M.: The Arctic oscillation signature in the
487 wintertime geopotential height and temperature fields, *Geophys. Res. Lett.*, 25,
488 1297-1300, <https://doi.org/10.1029/98GL00950>, 1998.
- 489 Wang, L., Chen, W., Huang, R. H., Interdecadal modulation of PDO on the impact of
490 ENSO on the east Asian winter monsoon, *Geophys. Res. Lett.*, 35, L20702,
491 <https://doi.org/10.1029/2008GL035287>, 2008.
- 492 Wu, R. G., and Wang, B., A Contrast of the East Asian Summer Monsoon–ENSO
493 Relationship between 1962–77 and 1978–93, *J. Climate*, 15, 3266-3279,
494 [https://doi.org/10.1175/1520-0442\(2002\)015<3266:ACOTEA>2.0.CO;2](https://doi.org/10.1175/1520-0442(2002)015<3266:ACOTEA>2.0.CO;2), 2002.
- 495 Wu, R. G.: Seasonal dependence of factors for year-to-year variations of South China
496 aerosol optical depth and Hong Kong air quality, *Int. J. Climatol.*, 34, 3204-3220,
497 <https://doi.org/10.1002/joc.3905>, 2014.
- 498 Wu, Z. W., Wang, B., Li, J. P., and Jin, F.-F.: An empirical seasonal prediction model of
499 the east Asian summer monsoon using ENSO and NAO, *J. Geophys. Res.*, 114,



- 500 D18120, <https://doi.org/10.1029/2009JD011733>, 2009.
- 501 Xie, S. P., Hu, K. M., Hafner, J., Tokinaga, H., Du, Y., Huang, G., and Sampe, T.: Indian
502 Ocean capacitor effect on Indo–Western Pacific climate during the summer
503 following El Niño, *J. Climate*, 22, 730-747,
504 <https://doi.org/10.1175/2008JCLI2544.1>, 2009.
- 505 Xue, F., and Liu, C. Z.: The influence of moderate ENSO on summer rainfall in eastern
506 China and its comparison with strong ENSO, 53, 791-800,
507 <https://xs.scihub.ltd/https://doi.org/10.1007/s11434-008-0002-5>, 2008.
- 508 Yang, Y., Liao, H., and Lou, S. J.: Decadal trend and interannual variation of outflow
509 of aerosols from East Asia: roles of variations in meteorological parameters and
510 emissions, *Atmos. Environ.*, 100, 141-153,
511 <https://doi.org/10.1016/j.atmosenv.2014.11.004>, 2015.
- 512 Yang, Y., Russell, L. M., Lou, S., Liao, H., Guo, J., Liu, Y., Singh, B., and Ghan, J.:
513 Dust-wind interactions can intensify aerosol pollution over eastern China, *Nature*
514 *Commun.*, 8, 15333, <https://xs.scihub.ltd/https://doi.org/10.1038/ncomms15333>,
515 2017.
- 516 Zhang, Q., Quan, J. N., Tie, X. X., Huang, M. Y., and Ma, X. C.: Impact of aerosol
517 particles on cloud formation: aircraft measurements in China, *Atmos. Environ.*, 45,
518 665-672, <https://doi.org/10.1016/j.atmosenv.2010.10.025>, 2011.
- 519 Zhang, R. H., Sumi, A., Kimoto, M.: Impact of El Niño on the East Asian Monsoon, *J.*
520 *Meteorol. Soc. Japan*, 74, 49-62, https://doi.org/10.2151/jmsj1965.74.1_49, 1996.



- 521 Zhao, S., Li, J., Sun, C.: Decadal variability in the occurrence of wintertime haze in
522 central eastern China tied to the Pacific Decadal Oscillation. *Scientific Reports*, 6,
523 27424, <https://xs.scihub.ltd/https://doi.org/10.1038/srep27424>, 2016.
- 524 Zheng, F., Li, J., Wang, L., Xie, F., and Li, X. F., Cross-seasonal influence of the
525 December–February Southern Hemisphere Annular Mode on March–May
526 meridional circulation and precipitation, *J. Climate*, 28, 6859–6881,
527 <http://dx.doi.org/10.1175/JCLI-D-14-00515.1>, 2015.
- 528 Zheng, F., Li, J., Li, Y. J., Zhao, S., and Deng, D. F., Influence of the summer NAO on
529 the spring-NAO-based predictability of the East Asian summer monsoon, *J. App.*
530 *Meteorol. Climatol.*, 55, <https://doi.org/10.1175/JAMC-D-15-0199.1>, 2016.
- 531 Zheng, F., Li, J. P., Kucharski, F., Ding, R. Q., and Liu, T.: Dominant SST Mode in the
532 Southern Hemisphere extratropics and its influence on atmospheric circulation.
533 *Adv. Atmos. Sci.*, 35, 881-895,
534 <https://xs.scihub.ltd/https://doi.org/10.1007/s00376-017-7162-7>, 2018.
- 535 Zhou, W., Wang, X., Zhou, T. J., Li, C., Chan, J. C. L.: Interdecadal variability of the
536 relationship between the East Asian winter monsoon and ENSO. *Meteorol. Atmos.*
537 *Phys.*, 98, 283-293, <https://doi.org/10.1007/s00703-007-0263-6>, 2007.
- 538 Zhu, J. L., Liao, H., and Li, J. P.: Increases in aerosol concentrations over eastern China
539 due to the decadal-scale weakening of the East Asian summer monsoon, *Geophys.*
540 *Res. Lett.*, 39(9), L09809, <https://doi.org/10.1029/2012GL051428>, 2012.
- 541



542 **Figure Captions:**

543 **Figure 1.** Spatial pattern of the (a) first empirical orthogonal function (EOF1) mode of
544 the monthly surface PM_{2.5} concentrations over China. (b) As in (a), but for the
545 second mode (EOF2). (c)-(d) As in (a)-(b), but for the column concentrations. The
546 numbers indicate fractional variance in the EOF modes.

547 **Figure 2.** (a) The first principal components (PC1) of the monthly PM_{2.5}
548 concentrations where the red and blue lines are for the surface and column
549 concentrations, respectively. (b) As in (a), but for PC2.

550 **Figure 3.** (a) Lead-lag correlation between the Niño3.4 index and PC1. Negative
551 (positive) lags indicate that the Niño3.4 index is leading (lagging) and the dashed
552 lines are the 0.05 significance levels. (b) As in (a), but for the correlation between
553 the NAOI and PC2. The red lines are based on the GEOS-4 meteorological fields,
554 and the blue lines are based on the observations.

555 **Figure 4.** Seasonal variations in the standard deviation of the (a) PC1, (b) PC2, (c)
556 Niño3.4 index, and (d) NAOI.

557 **Figure 5.** Spatial distribution of the correlation coefficients between the monthly sea
558 surface temperature and PC1 for PC1 lagging for (a) 3 months, (b) 2 months, (c)
559 1 month, and (d) simultaneous. Color shading indicates significance at the 0.05
560 level.

561 **Figure 6.** Spatial distribution of the correlation coefficients between the monthly sea
562 level pressure and PC2 of the (a) surface and (b) column PM_{2.5} concentrations.
563 Color shading indicates significance at the 0.05 level.



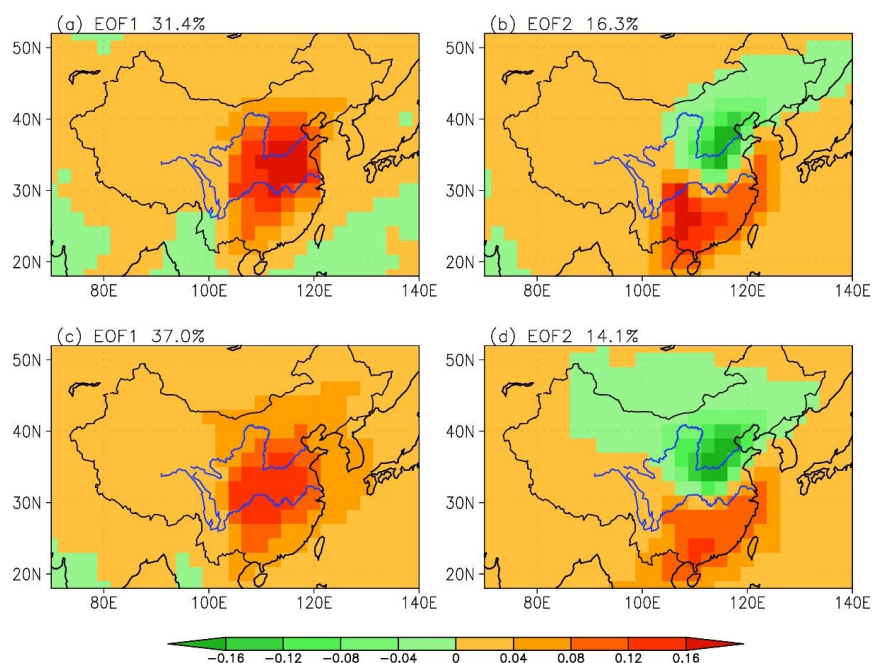
564 **Figure 7.** Spatial distribution of the correlation coefficients between the Niño3.4 index
565 and divergence at 700 hPa for the Niño3.4 index leading for 3 months. Color
566 shading indicates significance at the 0.05 level.

567 **Figure 8.** Regressions of the divergence at 300 hPa onto the simultaneous NAOI. Color
568 shading indicates significance at the 0.05 level.

569 **Figure 9.** Regressions of the planetary boundary layer height onto the (a) 3-month
570 leading Niño3.4 index and (b) simultaneous NAOI. Color shading indicates
571 significance at the 0.05 level.

572 **Figure 10.** Regressions of the skin temperature onto the (a) 3-month leading Niño3.4
573 index and (b) simultaneous NAOI. Color shading indicates significance at the 0.05
574 level.

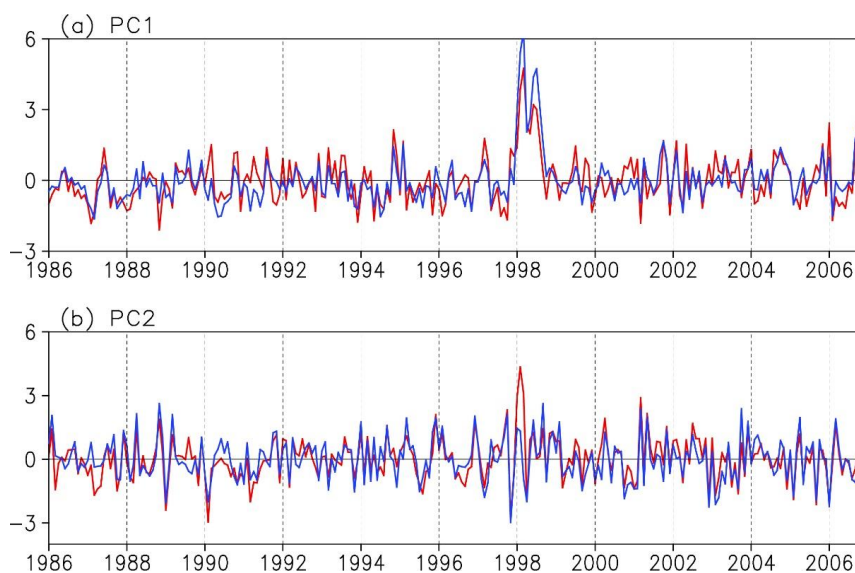
575



576

577 **Figure 1.** Spatial pattern of the (a) first empirical orthogonal function (EOF1) mode of
578 the monthly surface PM2.5 concentrations over China. (b) As in (a), but for the second
579 mode (EOF2). (c)-(d) As in (a)-(b), but for the column concentrations. The numbers
580 indicate fractional variance in the EOF modes.

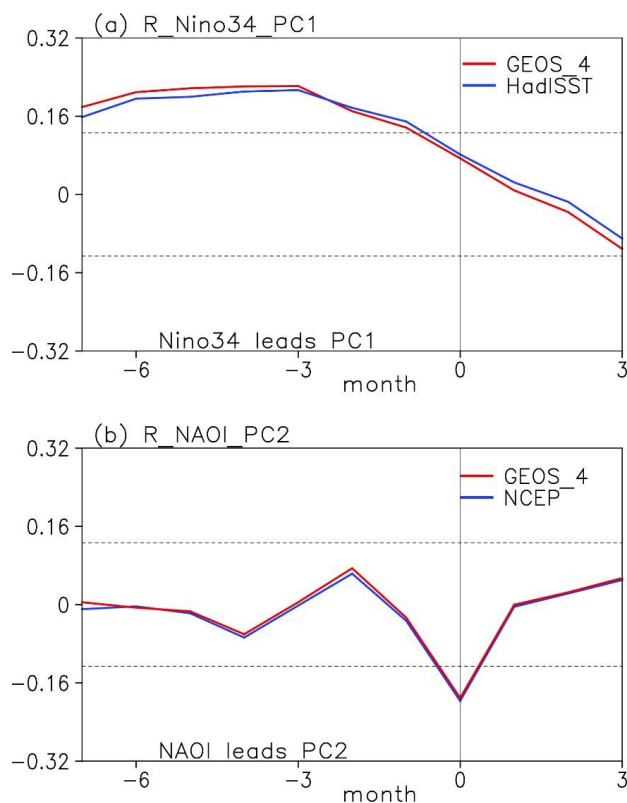
581



582

583 **Figure 2.** (a) The first principal components (PC1) of the monthly PM_{2.5}
584 concentrations where the red and blue lines are for the surface and column
585 concentrations, respectively. (b) As in (a), but for PC2.

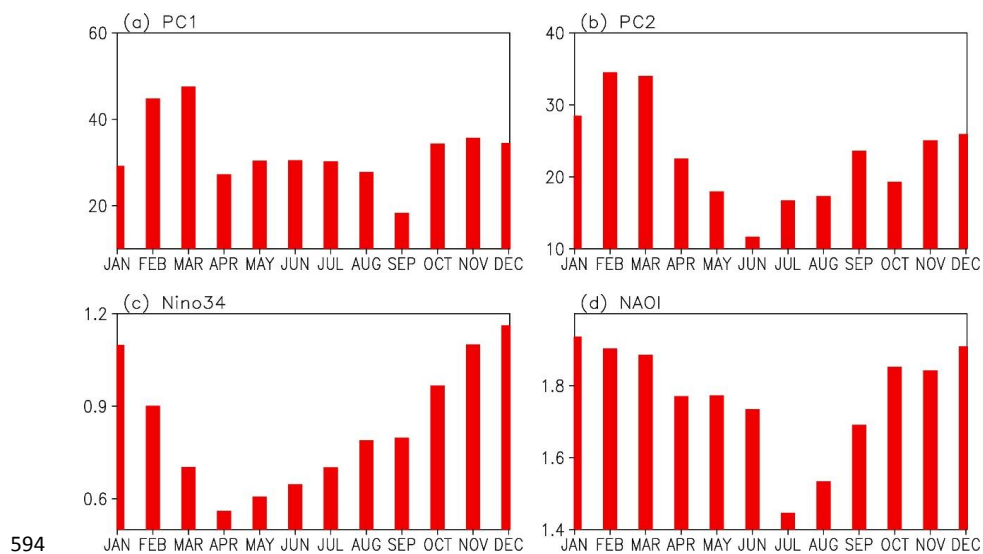
586



587

588 **Figure 3.** (a) Lead-lag correlation between the Niño3.4 index and PC1. Negative
589 (positive) lags indicate that the Niño3.4 index is leading (lagging) and the dashed lines
590 are the 0.05 significance levels. (b) As in (a), but for the correlation between the NAOI
591 and PC2. The red lines are based on the GEOS-4 meteorological fields, and the blue
592 lines are based on the observations.

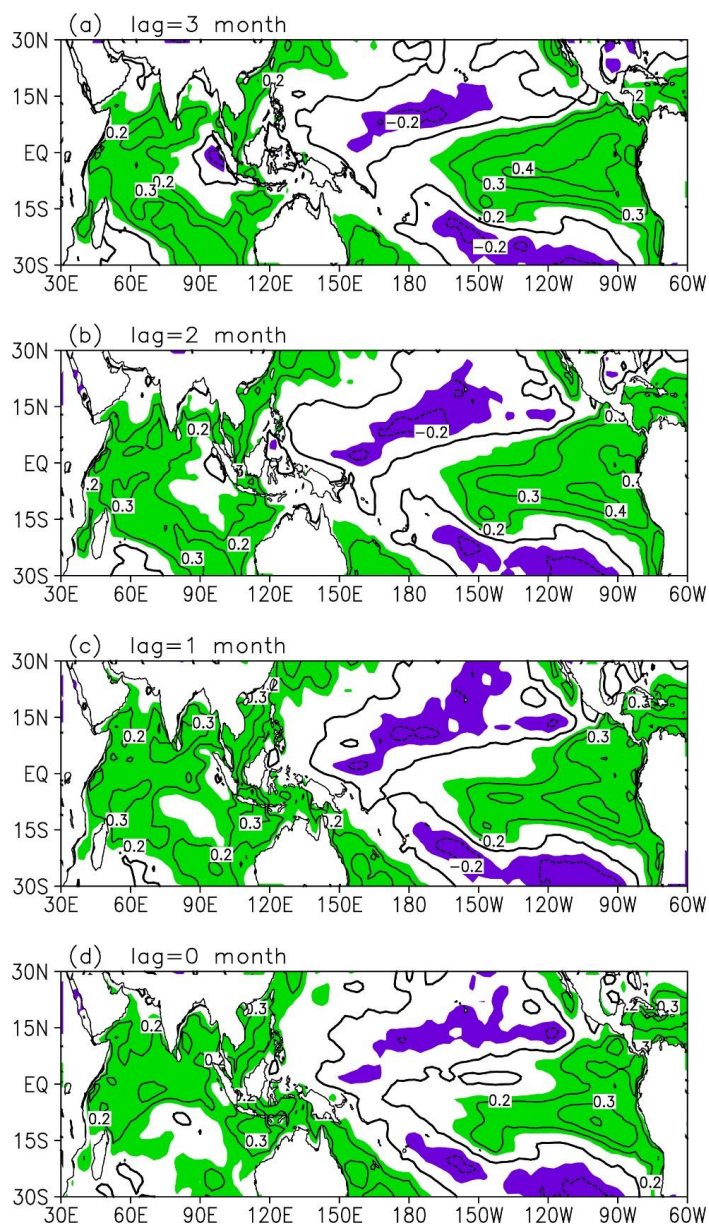
593



594

595 **Figure 4.** Seasonal variations in the standard deviation of the (a) PC1, (b) PC2, (c)
596 Niño3.4 index, and (d) NAOI.

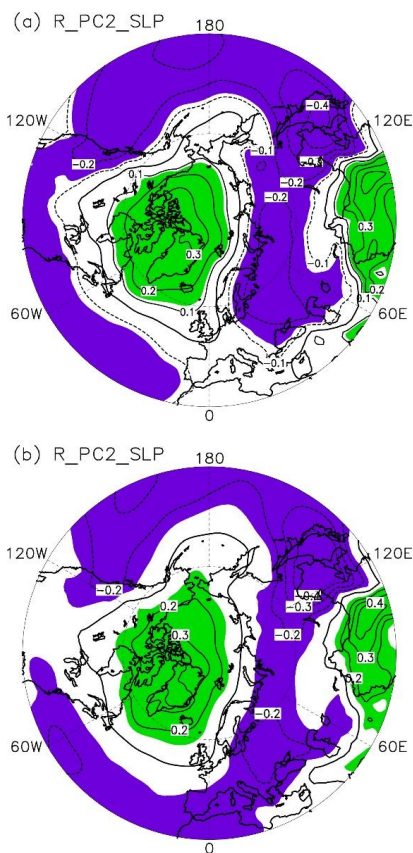
597



598

599 **Figure 5.** Spatial distribution of the correlation coefficients between the monthly sea
600 surface temperature and PC1 for PC1 lagging for (a) 3 months, (b) 2 months, (c) 1
601 month, and (d) simultaneous. Color shading indicates significance at the 0.05 level.

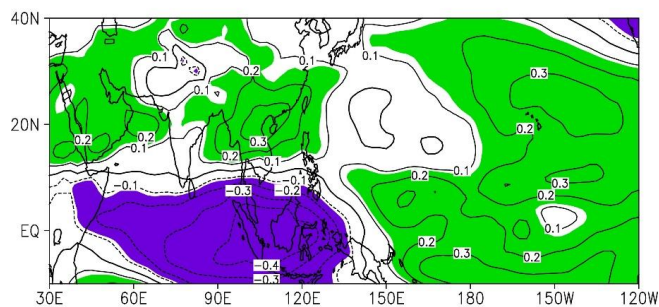
602



603

604 **Figure 6.** Spatial distribution of the correlation coefficients between the monthly sea
605 level pressure and PC2 of the (a) surface and (b) column PM_{2.5} concentrations. Color
606 shading indicates significance at the 0.05 level.

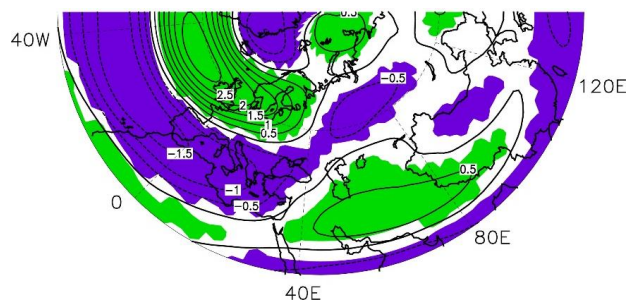
607



608

609 **Figure 7.** Spatial distribution of the correlation coefficients between the Niño3.4 index
610 and divergence at 700 hPa for the Niño3.4 index leading for 3 months. Color shading
611 indicates significance at the 0.05 level.

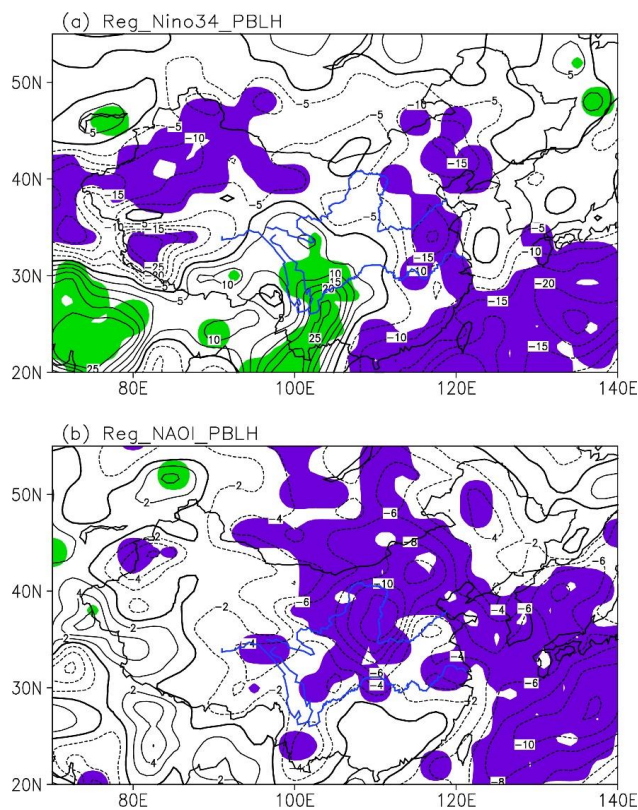
612



613

614 **Figure 8.** Regressions of the divergence at 300 hPa onto the simultaneous NAOI. Color
615 shading indicates significance at the 0.05 level.

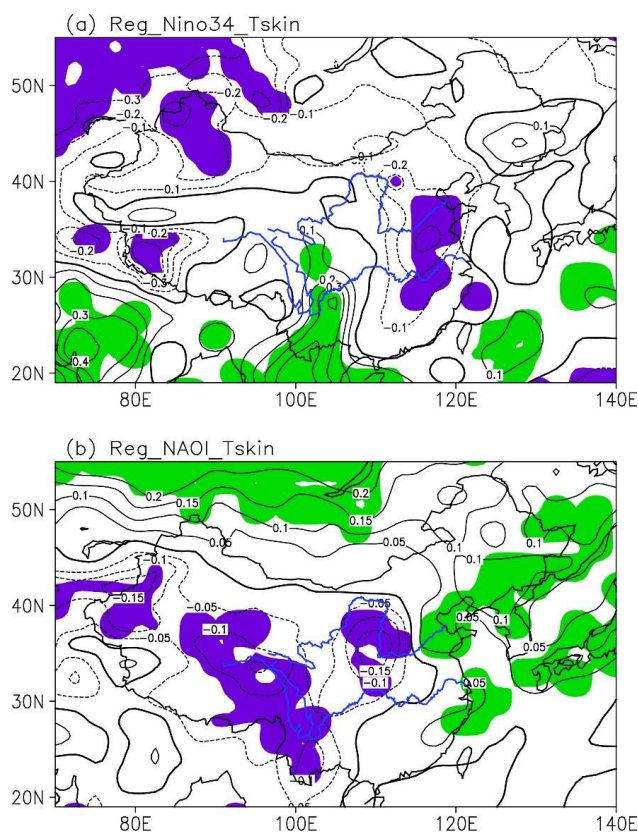
616



617

618 **Figure 9.** Regressions of the planetary boundary layer height onto the (a) 3-month
619 leading Niño3.4 index and (b) simultaneous NAOI. Color shading indicates
620 significance at the 0.05 level.

621



622

623 **Figure 10.** Regressions of the skin temperature onto the (a) 3-month leading Niño3.4
624 index and (b) simultaneous NAOI. Color shading indicates significance at the 0.05 level.